Supporting information for: Hydration dynamics of a peripheral membrane protein

Olivier Fisette,[†,‖] Christopher Päslack,[†,‡,‖] Ryan Barnes,[¶] J. Mario Isas,[§] Ralf Langen,[§] Matthias Heyden,[‡] Songi Han,[¶] and Lars V. Schäfer[*,†]

Center for Theoretical Chemistry, Ruhr-University, Bochum, Germany, Max-Planck Institut für Kohlenforschung, Mülheim an der Ruhr, Germany, Department of Chemistry and Biochemistry and Department of Chemical Engineering, University of California, Santa Barbara, U.S.A., and Department of Biochemistry and Molecular Biology, Zilkha Neurogenetic Institute, Keck School of Medicine, University of Southern California, Los Angeles, U.S.A.

E-mail: lars.schaefer@ruhr-uni-bochum.de

[*]To whom correspondence should be addressed
[†]RUB
[‡]MPK
[¶]UCSB
[§]USC
[‖]Contributed equally to this work

Details of MD simulations

Anx coordinates were taken from an X-ray crystal structure (PDB ID 1DM5)[S1] of the E105K variant; chain A from the homohexamer was retained, along with its two bound Ca^{2+} ions and crystal water molecules. The structure was subjected to 500 steps of steepest-descent (SD) energy minimization. A bilayer with 512 DOPC lipids was generated from a pre-equilibrated 128 DOPC bilayer by replicating the bilayer four-fold in the plane of the membrane. A DOPC/DOPS (7:3) bilayer was prepared from the DOPC bilayer, replacing the three terminal N-methyl groups (C13–C15) by hydrogens and the H12B atom by a carboxyl group (thus yielding the appropriate stereoisomer at the C12 position). An equal number of DOPC molecules from each leaflet was converted to DOPS; these molecules were chosen randomly and were evenly distributed in the membrane plane. The resulting system was energy-minimized (500 steps SD). A purely hydrophobic bilayer was prepared by setting all partial charges in the lipid molecules to zero. Harmonic position restraints (force constant 1000 kJ $mol^{-1}nm^{-2}$) were applied to the head group phosphorus and the terminal tail carbon atoms. To test the influence of the position restraints, a standard DOPC bilayer (i.e. with normal partial charges) was simulated with the same position restraints applied to the DOPC molecules. To test the influence of protein electrostatics, position-restrained (force constant 1000 kJ $mol^{-1}nm^{-2}$ on all protein non-hydrogen atoms) Anx with partial charges set to zero was simulated. For the Anx-on-membrane systems, Anx was then positioned atop the bilayer; the approximate initial insertion depth was chosen according to experimental results.[S2] After energy minimization (500 steps SD), all systems were solvated in identically-sized boxes ($135 \times 135 \times 115$ $Å^3$) that accommodate the protein, bilayer, and at least 20 Å of water above the protein in the dimension normal to the membrane. The minimum distance between Anx and its periodic image never dropped below 50 Å in any of our MD simulations, and hence the simulation box is sufficiently large. Random water molecules were then replaced by ions to neutralize the system. To test the influence of the counterion gradient, 120 mM ions were added to an additional Anx-on-DOPC-bilayer system. Total system sizes

were about 200 000 atoms.

Simulations were carried out with GROMACS 5.0.5.[S3,S4] The Amber99SB*-ILDNP protein forcefield,[S5–S10] Slipids forcefield[S11,S12] and TIP4P/2005[S13] water model were used. For one control system (see Table 1, main text), the TIP3P[S14] water model was used instead. The SETTLE[S15] and LINCS[S16] algorithms were applied to constrain the internal degrees of freedom of water molecules and the bonds in other molecules, respectively, allowing for a 2-fs integration time step. Short-range non-bonded Coulomb and Lennard-Jones 6-12 interactions were treated with a Verlet buffered pair list[S17] with potentials smoothly shifted to zero at a 10 Å cut-off. Long-range Coulomb interactions were treated with the PME method[S18] with a grid spacing of 1.2 Å and cubic spline interpolation. Analytical dispersion corrections were applied for energy and pressure to compensate for the truncation of the Lennard-Jones interactions. Periodic rectangular cells were used. The thermodynamic ensemble was nPT, except for systems including position-restrained lipids, where nVT was used instead, and except for the simulations that were used for the computation of the vibrational density of states, which were simulated in the nVE ensemble. In the nPT and nVT simulations, temperature was kept constant at 298 K by a velocity-rescaling thermostat[S19] with coupling time constant 0.1 ps. For constant 1.0 bar pressure, a Berendsen barostat[S20] was used with coupling time constant 0.5 ps and 4.5×10^{-5} bar^{-1} compressibility. The barostat was semi-isotropic for all lipid bilayer systems, and isotropic for those without lipids.

Analysis of protein position and stability

To investigate the binding of Anx to the membrane, we monitored the center-of-mass (COM) motion of the protein along the bilayer normal during the MD. We used the average position of the phosphate head groups of the upper leaflet to determine a reference point from which distances were measured. The distance of Anx to the membrane surface (Fig. S1A) increases until 30 ns and then fluctuates around an equilibrium value. We therefore considered the

first 30 ns of all simulations as additional equilibration time and excluded them from the analysis, unless otherwise noted.

To validate the membrane binding observed in our MD simulations, we compared the equilibrium position of Anx in our simulations to EPR measurements of fractional solvent accessibility (f_{SA})[S21] of residues 219 to 242. To do so, we counted the average number of water oxygens within 6.0 Å of each Anx residue during the last 70 ns of the trajectory for Anx on DOPC/DOPS bilayer (Fig. S1B). Residues 219, 222, 223, 227, 234, 235, 237, 238 and 239 were characterized as buried by EPR ($f_{SA} < 0.05$). These residues, except 227 located in a flexible loop, are also the least solvent-accessed ones in our simulations (below the dashed line in Fig. S1B). The general trend observed throughout the entire sequence is very similar between our MD simulations and the EPR experiment, indicating that the Anx position observed in our simulations is consistent with current knowledge. The binding mode of Anx onto phospholipid membranes is nonetheless a topic of active research,[S22] and our MD simulations do not take into account possible effects due to oligomerization[S23] and induced membrane curvature.[S21,S24] These processes, however, are unlikely to substantially change the altered water dynamics around the peripheral membrane protein.

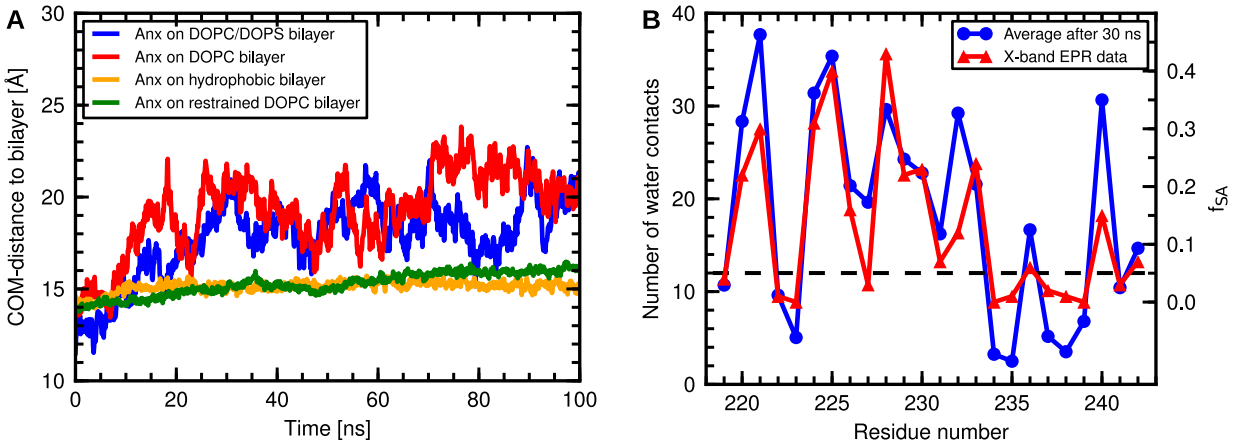

Figure S1: Anx position on bilayer. **A**: Time series of the COM distance of Anx to the phosphate head groups. **B**: Water accessibility of Anx residues 219 to 242 from MD (water oxygen within 6.0 Å) and EPR (f_{SA}).[S21]

After equilibration, the Anx-bound calcium ions establish salt bridges with the negatively-

charged carboxylate groups of the DOPS lipids. Experimentally, membrane binding of Anx is a calcium-dependent process[S25] that also requires negatively charged lipids. In our simulations, Anx remains bound even on a pure DOPC (zwitterionic lipid) bilayer because the timescale of dissociation is much longer than the simulation length. Anx is positioned on the bilayer at the start of the simulation, and thus remains stably bound for over 100 ns.

For all systems, the structural integrity of the protein was assessed from Cα-RMSD (Fig. S2). These were stable after 20 ns and remained essentially below 2.5 Å, with mean values ranging from 1.2 Å to 2.1 Å.

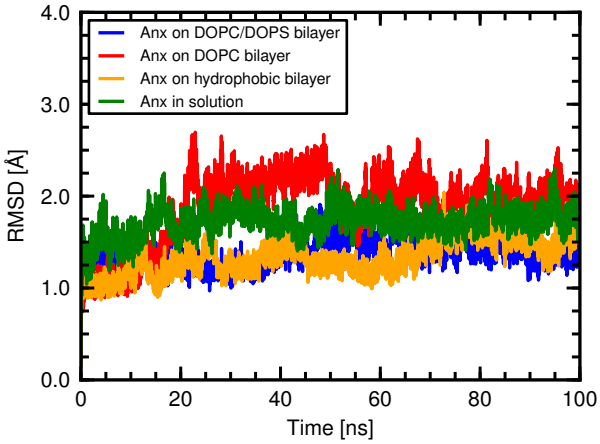

Figure S2: Cα-RMSD timeseries.

Water retardation from mean squared displacements

The retardation factors in Fig. 2 (main text) were computed from lateral MSDs of water molecules after 10 ps, which are plotted in Fig. S3. Retardation factors for additional control simulations are shown in Fig. S4. To assess the influence of considering 3D instead of 2D (lateral) translational motions, i.e., of including the component perpendicular to the membrane interface, water retardation factors for the Anx-on-DOPC/DOPS system were also computed from 3D MSDs (Fig. S4, magenta hexagons). The results are virtually identical to those for 2D translation (blue circles), indicating that lateral and perpendicular diffusion

are effectively slowed-down in similar ways by the membrane and the protein. Next, to investigate the influence of the water model, we repeated the Anx-on-DOPC/DOPS simulation with the TIP3P model (Fig. S4, red triangles; retardation factor computed relative to bulk TIP3P water). The trend is highly similar to that of the corresponding TIP4P/2005 simulations, although in terms of absolute numbers the diffusion of TIP3P is more than a factor of two faster than that of TIP4P/2005. Finally, to investigate whether (and, if so, by how much) the observed water dynamics depends on the position of Anx on the membrane, retardation factors were computed for the Anx on DOPC/DOPS system from trajectories initiated after only 5 ns of equilibration, i.e., *before* the protein COM position had stabilized (see Fig. S1A). The general trend is preserved (Fig. S4, green triangles), demonstrating that the water retardation is robust with respect to small changes in the actual position of the protein on the membrane. The protein-induced effect is smeared over a larger region and a clear plateau is harder to identify, though, since Anx position on the bilayer is not stable throughout the whole simulation.

Water dynamics around individual residues

Table S1 shows the water dynamics around eleven spin-labeled residues for Anx in solution measured by ODNP-enhanced NMR relaxometry. The corresponding retardation factors and their MD-derived counterparts are shown in Table S2. See also Fig. 3 in the main text.

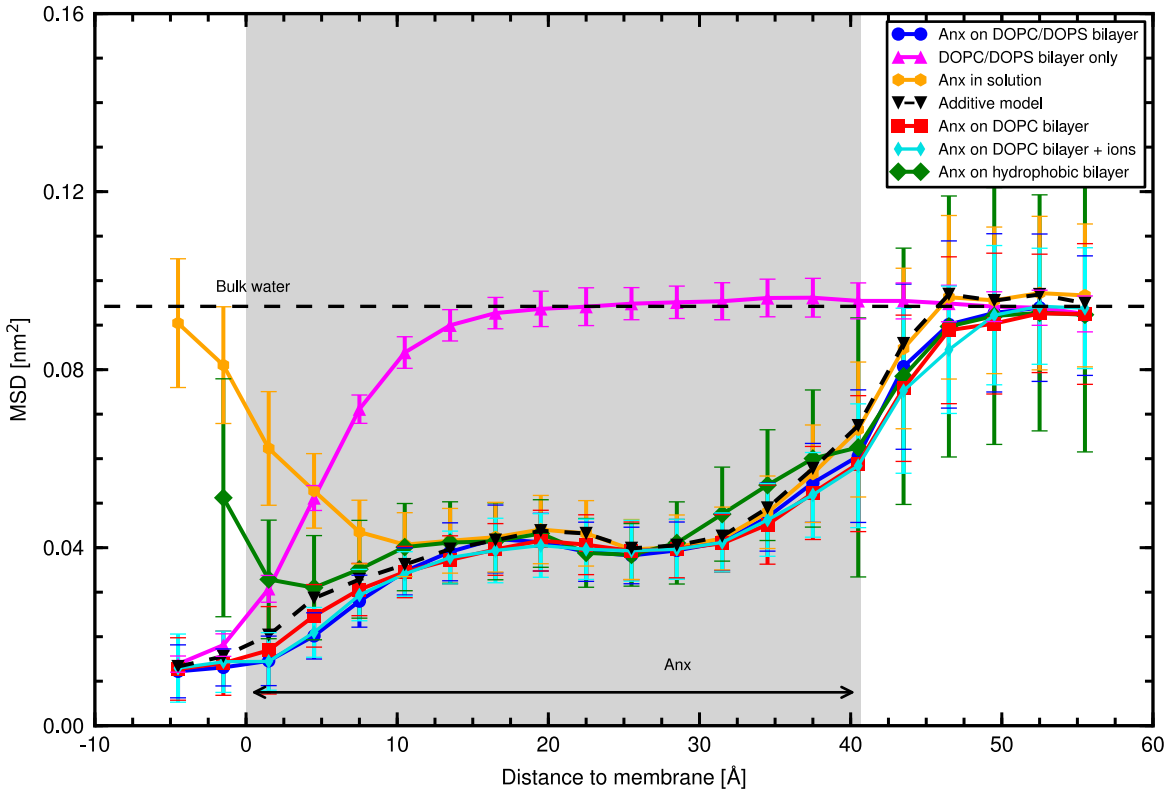

Figure S3: Lateral MSD of water around Anx as a function of distance to the phosphate head groups. Anx position on the membrane is indicated by the grey box. Vertical bars show standard deviations, reflecting the width of the underlying distribution. The statistical errors (not shown) are very small since the values are averaged over i) 14 independent simulations, and ii) several water molecules in each slab.

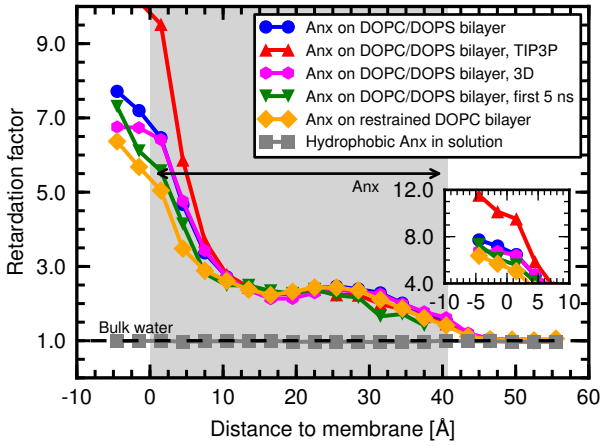

Figure S4: Water retardation around Anx as a function of distance to phosphate head groups in control simulations (see Table 1, main text).

Table S1: ODNP results. The values are given together with the standard deviations.

Residue	k_σ [$M^{-1}s^{-1}$]	k_ρ [$M^{-1}s^{-1}$]	$\xi \times 100$	τ [ps]
12	74.0 ± 8.4	746.0 ± 116.9	9.9 ± 1.9	181.9 ± 61.7
16	72.5 ± 4.2	870.6 ± 113.0	8.3 ± 1.2	210.2 ± 48.6
104	15.5 ± 0.7	647.3 ± 112.8	2.4 ± 0.4	503.7 ± 117.2
112	57.6 ± 10.0	1608.2 ± 249.8	3.6 ± 0.8	387.2 ± 124.5
121	63.7 ± 4.4	854.3 ± 340.2	7.5 ± 3.0	229.4 ± 161.1
124	25.7 ± 3.2	806.4 ± 109.1	3.2 ± 0.6	417.9 ± 102.6
137	39.1 ± 5.0	321.7 ± 90.6	12.2 ± 3.8	151.5 ± 93.5
141	59.2 ± 3.2	778.1 ± 191.8	7.6 ± 1.9	226.0 ± 92.9
162	52.4 ± 10.8	509.4 ± 36.6	10.3 ± 2.2	176.3 ± 68.7
180	35.1 ± 0.8	1188.8 ± 57.0	3.0 ± 0.2	440.0 ± 30.0
260	30.3 ± 4.6	219.3 ± 175.2	13.8 ± 11.2	133.9 ± 417.0

Table S2: Membrane distance (d) and local water retardation factors from MD* and ODNP for individual residues. The values are given together with the standard deviations.

Residue	d	Retardation factor					
		Anx on membrane			Anx in solution		
	Å	MD (5 Å)	MD (3 Å)	ODNP	MD (5 Å)	MD (3 Å)	ODNP
S12	36	1.7 ± 0.5	1.8 ± 0.3	6.4 ± 0.4	1.3 ± 0.5	1.2 ± 0.2	5.5 ± 1.9
R16	33	2.0 ± 0.6	2.7 ± 0.3	6.7 ± 0.4	1.2 ± 0.4	1.4 ± 0.2	6.4 ± 1.5
D104	9	12.9 ± 2.4	15.3 ± 2.0	15.5 ± 0.5	1.9 ± 0.4	2.2 ± 0.3	15.3 ± 3.6
L112	19	–	–	–	1.7 ± 0.5	1.4 ± 0.1	11.7 ± 3.8
N117	29	3.6 ± 0.8	4.0 ± 0.3	7.0 ± 0.4	–	–	–
H121	30	2.1 ± 0.6	2.9 ± 0.3	7.5 ± 0.3	1.3 ± 0.5	1.4 ± 0.2	7.0 ± 4.9
K124	26	4.0 ± 0.8	5.5 ± 0.6	9.2 ± 0.3	1.8 ± 0.4	1.9 ± 0.2	12.7 ± 3.1
K128	18	2.7 ± 0.8	3.3 ± 0.3	10.9 ± 0.6	–	–	–
K137	17	2.3 ± 0.6	2.8 ± 0.3	12.9 ± 0.4	1.4 ± 0.4	1.4 ± 0.2	4.6 ± 2.8
S141	9	5.7 ± 1.0	7.6 ± 0.9	15.1 ± 0.3	1.3 ± 0.4	1.4 ± 0.2	6.8 ± 2.8
S144	6	8.0 ± 1.4	10.5 ± 1.2	15.8 ± 0.4	–	–	–
D162	39	1.9 ± 0.5	2.4 ± 0.4	6.6 ± 0.4	1.4 ± 0.5	1.4 ± 0.3	5.3 ± 2.1
A180	18	7.4 ± 0.6	–	11.7 ± 0.3	2.3 ± 0.2	–	13.3 ± 0.9
L260	0	9.7 ± 1.3	11.1 ± 0.7	15.5 ± 0.5	1.2 ± 0.5	1.3 ± 0.1	4.1 ± 12.6

* Retardation factors measured for both 3- and 5-Å cut-offs

References

(S1) Cartailler, J. P.; Haigler, H. T.; Luecke, H. *Biochemistry* **2000**, *39*, 2475–2483.

(S2) Cheng, C.-Y.; Varkey, J.; Ambroso, M. R.; Langen, R.; Han, S. *Proc. Natl. Acad. Sci. U.S.A.* **2013**, *110*, 16838–16843.

(S3) Pronk, S.; Páll, S.; Schulz, R.; Larsson, P.; Bjelkmar, P.; Apostolov, R.; Shirts, M. R.; Smith, J. C.; Kasson, P. M.; van der Spoel, D.; Hess, B.; Lindahl, E. *Bioinformatics* **2013**, *29*, 845–854.

(S4) Páll, S.; Abraham, M.; Kutzner, C.; Hess, B.; Lindahl, E. In *Solving Software Challenges for Exascale*; Markidis, S., Laure, E., Eds.; Lecture Notes in Computer Science; Springer International Publishing, 2015; Vol. 8759; pp 3–27.

(S5) Cornell, W. D.; Cieplak, P.; Bayly, C. I.; Gould, I. R.; Merz, K. M.; Ferguson, D. M.; Spellmeyer, D. C.; Fox, T.; Caldwell, J. W.; Kollman, P. A. *J. Am. Chem. Soc.* **1995**, *117*, 5179–5197.

(S6) Wang, J.; Cieplak, P.; Kollman, P. A. *J. Comput. Chem.* **2000**, *21*, 1049–1074.

(S7) Hornak, V.; Abel, R.; Okur, A.; Strockbine, B.; Roitberg, A.; Simmerling, C. *Proteins* **2006**, *65*, 712–725.

(S8) Best, R. B.; Hummer, G. *J. Phys. Chem. B* **2009**, *113*, 9004–9015.

(S9) Lindorff-Larsen, K.; Piana, S.; Palmo, K.; Maragakis, P.; Klepeis, J. L.; Dror, R. O.; Shaw, D. E. *Proteins* **2010**, *78*, 1950–1958.

(S10) Aliev, A. E.; Kulke, M.; Khaneja, H. S.; Chudasama, V.; Sheppard, T. D.; Lanigan, R. M. *Proteins* **2014**, *82*, 195–215.

(S11) Jämbeck, J. P. M.; Lyubartsev, A. P. *J. Phys. Chem. B* **2012**, *116*, 3164–3179.

(S12) Jämbeck, J. P. M.; Lyubartsev, A. P. *J. Chem. Theory Comput.* **2012**, *8*, 2938–2948.

(S13) Abascal, J. L. F.; Vega, C. *J. Chem. Phys.* **2005**, *123*, 234505.

(S14) Jorgensen, W. L.; Chandrasekhar, J.; Madura, J. D.; Impey, R. W.; Klein, M. L. *J. Chem. Phys.* **1983**, *79*, 926–935.

(S15) Miyamoto, S.; Kollman, P. A. *J. Comput. Chem.* **1992**, *13*, 952–962.

(S16) Hess, B. *J. Chem. Theory Comput.* **2008**, *4*, 116–122.

(S17) Páll, S.; Hess, B. *Comput. Phys. Commun.* **2013**, *184*, 2641 – 2650.

(S18) Essmann, U.; Perera, L.; Berkowitz, M. L.; Darden, T.; Lee, H.; Pedersen, L. G. *J. Chem. Phys.* **1995**, *103*, 8577–8593.

(S19) Bussi, G.; Donadio, D.; Parrinello, M. *J. Chem. Phys.* **2007**, *126*, 014101.

(S20) Berendsen, H. J. C.; Postma, J. P. M.; van Gunsteren, W. F.; DiNola, A.; Haak, J. R. *J. Chem. Phys.* **1984**, *81*, 3684–3690.

(S21) Isas, J. M.; Kim, Y. E.; Jao, C. C.; Hegde, P. B.; Haigler, H. T.; Langen, R. *Biochemistry* **2005**, *44*, 16435–16444.

(S22) Chen, Z.; Mao, Y.; Yang, J.; Zhang, T.; Zhao, L.; Yu, K.; Zheng, M.; Jiang, H.; Yang, H. *Proteins* **2014**, *82*, 312–322.

(S23) Langen, R.; Isas, J. M.; Luecke, H.; Haigler, H. T.; Hubbell, W. L. *J. Biol. Chem.* **1998**, *273*, 22453–22457.

(S24) Isas, J. M.; Langen, R.; Hubbell, W. L.; Haigler, H. T. *J. Biol. Chem.* **2004**, *279*, 32492–32498.

(S25) Swairjo, M. A.; Concha, N. O.; Kaetzel, M. A.; Dedman, J. R.; Seaton, B. A. *Nat. Struct. Biol.* **1995**, *2*, 968–974.